DNA Damage and Repair

Molecular Cancer Research

Alternative NHEJ Pathway Components Are Therapeutic Targets in High-Risk Neuroblastoma

Erika A. Newman[1], Fujia Lu[1], Daniela Bashllari[1], Li Wang[2], Anthony W. Opipari[3], and Valerie P. Castle[2]

Abstract

In neuroblastoma, *MYCN* genomic amplification and segmental chromosomal alterations including *1p* or *11q* loss of heterozygocity and/or *17q* gain are associated with progression and poor clinical outcome. Segmental alterations are the strongest predictor of relapse and result from unbalanced translocations attributable to erroneous repair of chromosomal breaks. Although sequence analysis of affected genomic regions suggests that these errors arise by nonhomologous end-joining (NHEJ) of DNA double-strand breaks (DSB), abnormalities in NHEJ have not been implicated in neuroblastoma pathogenesis. On this basis, the hypothesis that an error-prone mechanism of NHEJ is critical for neuroblastoma cell survival was tested. Plasmid-based DSB repair assays demonstrated efficient NHEJ activity in human neuroblastoma cells with repair products that were error-prone relative to nontransformed cells. Neuroblastoma cells derived from tumorigenic neuroblastic phenotypes had differential DNA repair protein expression patterns compared with nontumorigenic cells. Tumorigenic neuroblastoma cells were deficient in DNA ligase IV (Lig4) and Artemis (DCLRE1C), mediators of canonical NHEJ. Conversely, enzymes required for an error-prone alternative NHEJ pathway (alt-NHEJ), DNA Ligase IIIα (Lig3), DNA Ligase I (Lig1), and PARP1 protein were upregulated. Inhibition of Lig3 and Lig1 led to DSB accumulation and cell death, linking alt-NHEJ to cell survival in neuroblastoma. Neuroblastoma cells demonstrated sensitivity to PARP1 inhibition (PARPi) that paralleled PARP1 expression. In a dataset of human neuroblastoma patient tumors, overexpression of genes encoding alt-NHEJ proteins associated with poor survival.

Implications: These findings provide an insight into DNA repair fidelity in neuroblastoma and identify components of the alt-NHEJ pathway as promising therapeutic targets. *Mol Cancer Res; 13(3); 470–82. ©2015 AACR.*

Introduction

Neuroblastoma, the most common extracranial solid tumor in children, arises from neural crest precursors in the adrenal medulla and sympathetic neural ganglia. Nearly 50% of patients have high-risk disease that is refractory or relapse despite multimodality therapy. Such cases are commonly characterized by older age at presentation, tumor cell diploidy, and by recurrent chromosomal imbalances that predict prognosis. Amplification of *MYCN* (MNA) is associated with rapid tumor progression and advanced stage disease (1, 2). Segmental chromosomal alterations frequently occur in older children with stage IV tumors and are the strongest predictors of relapse, indicating a role in neuroblastoma pathogenicity (3, 4). The most common alterations require DNA double-strand breaks (DSB) resulting in segmental deletions of *1p*, *3p*, *4p*, or *11q* and/or gain of *17q*, *1q*, and *2p* regions (5–10). Affected breakpoints have no DNA sequence similarities and result from unbalanced translocations generated by erroneous repair of DSB (11). Sequence analysis of recurrent breakpoint regions in neuroblastoma tumors provides evidence that segmental errors are generated by a DSB repair mechanism with characteristics of non-homologous end-joining (NHEJ; refs. 11, 12). This implies that segmental alterations could represent either an intact NHEJ mechanism processing abnormally high numbers of DSB or an underlying abnormality of DNA repair and maintenance (13).

The two major DSB repair pathways are homologous recombination (HR) and NHEJ. Compared with HR, NHEJ is functional throughout the cell cycle and restores chromosomal continuity without sequence homology (14, 15). There are two major processes of NHEJ that differ with respect to repair factors and end-joining fidelity. In canonical form, classical NHEJ (c-NHEJ) is critical for genomic stability and is mediated by DNA repair factors DNA-PKcs, Ku70/Ku86, Artemis (DCLRE1C), XLF/Cernunnos, DNA Ligase IV (Lig4), and XRCC4. Despite its nonconservative nature, c-NHEJ is required to suppress translocation formation and generally restores chromosome integrity without rearrangements (16). In addition to c-NHEJ, an alternative NHEJ (alt-NHEJ) mechanism has been described which relies on a

[1]Department of Surgery, C.S. Mott Children and Women's Hospital, Translational Oncology Program, The University of Michigan Medical School, Ann Arbor, Michigan. [2]Department of Pediatrics, C.S. Mott Children and Women's Hospital, Translational Oncology Program, The University of Michigan Medical School, Ann Arbor, Michigan. [3]Department of Obstetrics and Gynecology, C.S. Mott Children and Women's Hospital, The University of Michigan Medical School, Ann Arbor, Michigan.

Note: Supplementary data for this article are available at Molecular Cancer Research Online (http://mcr.aacrjournals.org/).

Corresponding Author: Erika A. Newman, C.S. Mott Children and Women's Hospital, 1040 East Hospital Drive, Ann Arbor, MI 48109. Phone: 734-764-6482; Fax: 734-232-8667; E-mail: eanewman@med.umich.edu

doi: 10.1158/1541-7786.MCR-14-0337

distinct set of repair factors (17–19). PARP1, together with DNA Ligase IIIα (Lig3) or DNA Ligase I (Lig1) binds DSB and initiates end-joining via an alt-NHEJ mechanism that does not utilize c-NHEJ factors (20–22). Rather than break end synapsis via c-NHEJ, alt-NHEJ is distinguished by low fidelity end-joining with frequent microhomologies, relying on base–pairing interactions at direct repeats flanking the DSB (23). The hallmark of alt-NHEJ is a more error-prone repair characterized by deletions and unbalanced translocations (24). The viewpoint that alt-NHEJ is the major DNA repair pathway to pathogenic chromosomal errors is further strengthened by the finding that c-NHEJ–deficient mice develop tumors with chromosomal translocations generated by alt-NHEJ (16, 25). This implies that the low fidelity alt-NHEJ repair mechanism has critical function in cancer cell survival and in tumor progression.

The tendency of high-risk neuroblastoma tumors to harbor segmental alterations generated by a repair process with hallmarks of NHEJ prompted us to test the hypothesis that neuroblastoma cells survive by an alt-NHEJ mechanism to overcome DSB. Here, we performed a detailed analysis of NHEJ features in neuroblastoma to determine whether erroneous DNA end-joining is a critical pathogenic mechanism for this pediatric cancer. Utilizing both neuroblastic and stromal-like human neuroblastoma cells with diverse cytogenetic features reflecting the heterogeneity of neuroblastoma tumors, we find evidence that DSB repair occurs by alt-NHEJ. Our analysis reveals a surprising deficiency of c-NHEJ components with upregulation of alt-NHEJ repair factors in neuroblastoma cells with high-risk genotypes. We show that alt-NHEJ sustains viability in neuroblastoma cells and discover an important clinical association between alt-NHEJ pathway gene expression and patient survival. These data offer new insights into DNA repair capacity of high-risk neuroblastoma and pave the way for novel studies targeting alt-NHEJ in neuroblastoma tumors.

Materials and Methods

Cell culture

Human neuroblastoma cell lines SH-EP1, SH-SY5Y, LAI-55n, IMR32, SK-N-Be(2), and two fibroblast cell lines I and II (IMR90 and HFF-1) were grown in minimal essential medium, supplemented with 10% FBS, 2 mmol/L glutamine, 100 U/mL penicillin, and 100 μg/mL streptomycin (all from Life Technologies). The stably transfected cell line SH-EP1-MYCN also contained G418 as a selection agent. IMR32 medium was further supplemented with 1 mmol/L pyruvate and 0.075% $NaHCO_3$ and all were placed in a 5% CO_2 incubator at 37°C. Cell lines were obtained from ATCC, with the exception of LAI-55n cells, which were obtained from Sigma-Aldrich. In July of 2014, cells were sent to IDEXX RADIL BioResearch for authentication using CellCheck 9, which checks for eight short tandem repeat markers and amelogenin. The genetic profiles of each cell line were then confirmed by comparing with established reference profiles.

NHEJ and HR plasmid assay

NHEJ and HR reporter plasmids were obtained as generous gifts from the laboratory of Dr. Vera Gorbunova, The University of Rochester (Rochester, NY). The reporter plasmids were linearized by I-SceI or HindIII restriction enzymes and purified using Qiagen purification kit. Exponentially growing cells were transfected with linearized reporter plasmids, using TransIT-LT1 reagent (Mirus) according to the manufacture protocol. The same amount of NHEJ-GFP and HR-GFP, which are the DSB repair products of NHEJ and HR reporter plasmids, were used as positive controls for 100% repair. DSB repair plasmids were cotransfected with DSRed expressing plasmids to control for transfection difference among cell lines. The gating for GFP^+ and $DsRed^+$ cells was determined in each experiment by cells transfected with GFP, DsRed, or negative control plasmids. To increase transfection efficiency, a same-day plating strategy was used. More than 30,000 cells were analyzed for each experiment. On the pGFP-Pem1 plasmid, there is a unique enzyme digestion site for BsrG1 in the first exon of GFP, and a unique enzyme digestion site for HindIII in the intron of GFP (Pem1). Therefore, BsrG1-digested pEGFP-Pem1 was used to measure accuracy of NHEJ repair and HindIII-digested pEGFP-Pem1 was used to measure overall repair activity. Significant differences were analyzed with two-way ANOVA and with the Student t test (significant at $P < 0.05$).

Cell viability assays

Cell viability was determined by the 3-(4,5-dimethylthiazol-2-yl)-2,5-diphenyl-tetrazolium bromide (MTT) assay according to the manufacturer's instructions (Sigma-Aldrich, M5655). Neuroblastoma cells and fibroblasts were plated in triplicate at 5×10^3 to 1×10^4 cells/well in 96-well culture plates in MEM. On the following day, cells were treated either with inhibitors or siRNA as described below. At the endpoint, treated cells were incubated with MTT dye (1 mg/mL) at 37°C for 4 hours and lysed in a buffer containing 20% (w/v) N,N-dimethylformamide (pH 4.5). Absorbance at 570 nmol/L (OD_{570}) was determined for each well using an ELX 808 automated microplate reader (Biotech Instruments). After subtraction of background absorbance, the OD_{570} of treated cells was divided by that of untreated cells to obtain the percentage of viable cells. In some experiments, cell viability was determined by Trypan blue exclusion. For these assays, cells (2×10^5 cells/well) were plated on 24-well plates and treated with either inhibitor or siRNA. After variable times, cells were harvested by trypsinization, washed with PBS, resuspended in MEM containing 0.2% Trypan blue (Invitrogen), and counted (living and dead) by light microscopy. Significant differences were analyzed with two-way ANOVA ($P < 0.05$).

Western blot analysis

Whole-cell extracts were prepared using the RIPA lysis buffer system (Santa Cruz Biotechnology) and protein concentrations were measured using BSA as standard using the Bradford Bio-Rad protein assay (Bio-Rad). Thirty-five micrograms of protein were resolved by SDS-PAGE and transferred onto PVDF membrane (Millipore). Blocking was done with 5% milk in TBST for one hour at room temperature, primary antibodies were diluted in 5% milk and incubated overnight at 4°C, and secondary antibodies were diluted in 5% milk and incubated for one hour at room temperature. Primary antibodies used were Lig3 (ab587 Abcam), Lig1 (ab615 Abcam), PARP1 (sc-8007 Santa Cruz Biotechnology), Lig4 (sc-28232 Santa Cruz Biotechnology), Artemis (ab3834 Abcam), Ku70 (sc-5309 Santa Cruz Biotechnology), and Ku80 (sc-9034 Santa Cruz Biotechnology), RAD51 (sc-8349 Santa Cruz Biotechnology), and RAD54 (sc-11428 Santa Cruz Biotechnology). Western Blot analyses were visualized using enhanced chemiluminescence (Amersham). Protein expression was quantified utilizing ImageJ software (http://imagej.nih.gov/ij/). The

heatmap plot was based on protein expression quantification, and was generated using conditional formatting in MS Excel. For each protein, the highest expression was set to a maximum of 1 (red) and lowest expression set to zero (green). For visual comparison, DNA repair protein expression levels were set as fractions of the maximum for each cell line. Experiments were repeated six times. Significant expression differences were analyzed with two-way ANOVA ($P < 0.05$).

L67 and PARP1 inhibitor treatment

The Lig3/Lig1 inhibitor L67 was obtained as a generous gift from Dr. Alan Tomkinson The University of New Mexico and PARP1 inhibitor BYK204165 was purchased from Sigma-Aldrich. Neuroblastoma cells and normal fibroblasts were cultured in 96-well culture plates at 5×10^3 to 1×10^4 cells/well. On the following day, cells were treated with L67 (0, 1, 5, 10 μmol/L) or BYK (0, 5, 10 μmol/L). On day 3, cell viability was evaluated by the MTT assay. Experiments were repeated three times and significant differences were analyzed with two-way ANOVA ($P < 0.05$).

Immunofluorescent microscopy and quantification of γH2AX

Neuroblastoma cells and controls were seeded in chamber slides. At different time points following treatment with L67 or BYK, cells were fixed with 4% paraformaldehyde for 15 minutes, washed with PBS, and permeabilized in 0.2% Triton-X100. After blocking with 5% normal goat serum (NGS) for one hour, samples were incubated with anti-phospho-histone γH2AX (Ser139) mouse monoclonal antibody (clone JBW301; Millipore) at a 1:500 dilution in 2.5% NGS-PBS overnight at 4°C, followed by incubation with the secondary antibody Alexa Fluor 488 goat anti-mouse-IgG (1:1000) for 1 hour. Cells were then washed with PBS and mounted using mounting solution with DAPI (Invitrogen). Images of γH2AX foci and nuclei were taken using a Leica DMR fluorescent microscope at ×40. Quantitative analysis of foci was carried out using ImageJ software. To test for variation between experiments, 400 to 500 cells from three different experiments were scored for each data point. The mean number of foci per nucleus and the SD from three independent measures were calculated.

FITC annexin V detection

SH-SY5Y and IMR32 cells were cultured in 6-well plates at 2×10^5 cells/well. On the following day, cells were treated with L67 (48 hours) or BYK (48 hours). Cells were then collected and stained with FITC Annexin V and propidium iodide (PI), followed by flow-cytometric analysis according to the manufacturer's protocol (BD Pharmingen, 556547).

siRNA-mediated silencing

SH-SY5Y, SH-EP1, and IMR32 cells were plated at a density of 2×10^6 cells per 10-cm culture plate. On the following day, cells were transfected with SMART-pool Lig3 siRNA (Dharmacon, Inc) using a Nucleofactor transfection reagent (Amaxa), as per the manufacturer's protocol. siGlo (Dharmacon) were cotransfected to measure transfection efficiency. Mock transfection and transfection with scrambled siRNA served as controls. Seventy-two hours later, cells were harvested and successful depletion by Lig3 siRNA was confirmed by Western blot analysis using Lig3 antibodies.

Public dataset gene expression analysis

Academic Medical Center cohort; Gene Expression Omnibus (GEO) database accession no. GSE16476 (http://r2.amc.nl) was utilized to study gene expression of alt-NHEJ ligases (Lig3, Lig1), PARP1, and Lig4 in previously analyzed cohorts of neuroblastoma tumor samples (26). Data as shown were analyzed and downloaded from the website, formatted for publication. Expression cutoff for each repair gene was determined by the R2 Kaplan–Meier Scanner. Scan modus was used for cutoff determination with a minimum group size of 10 to determine the best *P* values, and *P* values were corrected for multiple testing (Bonferroni).

Results

An erroneous mechanism of NHEJ is the dominant DSB repair pathway in neuroblastoma cells

Neuroblastoma tumors harbor segmental chromosomal alterations that are thought to arise from misrepair of DSB by the DNA end-joining process. It is not known whether DSB repair pathways are affected in neuroblastoma tumors. We set out to examine the frequencies of DNA end-joining in a panel of neuroblastoma cells and tested whether DSB repair efficiency was altered compared with normal cells. Plasmid-based reporter assays provide a reliable method to assess DSB repair, quantifying repair efficiency and fidelity of the end-joining process (27). Induction of DSB within a *GFP* reporter cassette by restriction enzyme digestion produces broken DNA ends that initiate a wide spectrum of cellular repair events that restore GFP expression (Supplementary Fig. S1; refs. 15, 27, 28). Restriction enzymes, including Hind III, I-SceI, or BsrG1 induced DSB in reporter cassettes, which were utilized to quantify DSB repair activity in neuroblastoma cells of varying cytogenetic phenotypes. We examined a diverse panel of human neuroblastoma cell lines derived from invasive neuroblastic tumors with chromosomal alterations frequently found in neuroblastoma. SK-N-Be2, IMR32, and LAI-55n are neuroblastic neuroblastoma cell lines with MNA and *1p* deletion, biologic features of advanced disease (29). To represent heterogeneity of neuroblastoma tumors (Supplementary Table S1), repair features in these high-risk cells were compared with nontumorigenic stromal-like neuroblastoma cells that resemble fibroblasts (SH-EP1) and with nontransformed human cells (fetal lung fibroblasts and neonatal foreskin fibroblasts) as normal controls.

We first analyzed efficiencies of NHEJ and HR DSB repair events to determine the predominant end-joining mechanism utilized by neuroblastoma cells. Although NHEJ is the predominant DSB repair pathway in mammalian cells, HR efficiency is increased in various cancer cells, particularly sporadic breast cancer compared with normal cells (28). Exponentially growing cells were transfected with linearized NHEJ (cut with HindIII or I-SceI) or HR (cut with I-SceI) reporter plasmids. DSB repair plasmids were cotransfected with DSRed expressing plasmids to control for differences in transfection efficiency among cell lines. Digestion with HindIII in NHEJ plasmid leaves compatible broken DNA ends, whereas I-SceI digestion produces incompatible ends. The rationale for selecting two distinct restriction sites was that radiation and chemotherapy medications cause nonspecific DSBs that are more likely to have incompatible ends, therefore NHEJ-I-SceI may resemble repair occurring after cancer therapies (15). NHEJ and HR reporters have been validated by plasmid rescue and

sequencing studies (27, 28). Repair efficiency, meaning the fraction of linearized plasmids rejoined, was measured by quantification of GFP expression using flow cytometry.

Compared with HR, NHEJ was the predominant DSB rejoining mechanism in neuroblastoma cell lines tested, including SH-EP1, SK-N-Be(2), IMR32, and LAI-55n cells (Fig. 1A). In neuroblastoma cells, NHEJ efficiencies detected were significantly higher than HR efficiencies indicating that NHEJ is the preferred DSB repair pathway in neuroblastoma cells ($P < 0.0001$). Nontransformed controls tested demonstrated low overall repair efficiencies and there were no significant differences detected between HR and NHEJ activity ($P = 0.07$). NHEJ-Hind III and NHEJ-ISceI showed similar NHEJ repair activity indicating that the same end-joining mechanism was likely responsible for repair of both compatible and incompatible DNA ends. We next evaluated whether the level of NHEJ activity differed between neuroblastoma cells with high-risk genotypes, stromal-like cells, and fibroblasts (Fig. 1B). There was clear NHEJ repair efficiency advantage in SK-N-Be2, IMR32, and LAI-55n cells compared with SH-EP1 and nontransformed cells ($P < 0.0001$). SK-N-Be2, IMR32, and LAI-55n cells were derived from advanced neuroblastoma tumors that harbor chromosomal alterations thought to have a role in tumor pathogenesis (MNA and *1p* deletion). These data indicate that these more high-risk neuroblastoma cells have highly efficient levels of endogenous NHEJ activity compared with stromal-like SH-EP1 cells and nontransformed human fibroblasts.

Fidelity of repair was separately measured using an endonuclease that required precise restriction site repair. BsrG1 recognizes a restriction site within the exon of the *GFP* gene therefore only accurate repair of BsrG1-digested reporter plasmid generates intact GFP protein. Conversely, restriction sites for HindIII are outside of the coding region and are permissive of microdeletion or addition of bases during the end-joining process (Supplementary Fig. S2; ref. 27). Accuracy of repair was represented by the ratio of GFP fluorescence generated by BsrG1-digested NHEJ plasmid to fluorescence generated by plasmid digested with HindIII. This measure of accuracy was lower in neuroblastoma cells compared with nontransformed controls (Fig. 1C). This finding indicates that compared with normal fibroblasts, NHEJ repair in neuroblastoma cells is more likely to generate DSB repair errors. The analysis suggests that neuroblastoma end-joining products are highly error-prone with repair error frequencies ranging from 30% to 45% versus 0% to 5% in nontransformed controls.

In all, *GFP* plasmid-based DSB repair assays demonstrate that NHEJ is the dominant DNA repair pathway in neuroblastoma cells. There are differences in NHEJ repair activity between neuroblastic cells with high-risk genotypes and stromal-like SH-EP1 cells, with SK-N-Be2, IMR32, and LAI-55n having the highest repair efficiencies. Compared with nontransformed cells, NHEJ activity in neuroblastoma cells results in end-joining products that are more prone to DSB repair errors. These data provide new insight into NHEJ repair capacity in neuroblastoma cells and suggests that NHEJ activity may be altered.

Neuroblastoma cells have a differential NHEJ protein expression pattern

The two known biochemical mechanisms of NHEJ differ with respect to end-joining fidelity and require different DNA-binding proteins and ligases to complete the DSB repair process. Given the high NHEJ repair efficiencies detected in neuroblastoma cells with high-risk genotypes, we next examined expression of DSB-binding proteins by Western blot analysis in a broader panel of neuroblastic neuroblastoma cells with segmental chromosomal alterations commonly found in neuroblastoma tumors (Supplementary Table S1). To determine which end-joining factors were representative of NHEJ activity in neuroblastoma, SK-N-Be(2), IMR32, LAI-55n (neuroblastic, MNA, and 1p deletion), and SH-SY5Y (neuroblastic, *1q* trisomy) cells were compared with normal fibroblasts and SH-EP1 cells.

The analysis revealed a distinct pattern of NHEJ protein expression in neuroblastoma cells with high-risk genotypes (Fig. 2A and Supplementary Fig. S3). SH-SY5Y, SK-N-Be(2), IMR32, and LAI-55n cells expressed significantly high protein levels of Lig3, Lig1, and PARP1 compared with fibroblasts and SH-EP1 cells. Each of these proteins are components of the alt-NHEJ repair pathway. SH-EP1 cells and fibroblasts had low expression of all three alt-NHEJ proteins tested (Lig3, Lig1, and PARP1). Interestingly, we also found that the MNA cell lines IMR32 and LAI-55n were significantly deficient in Lig4 compared with all of the other cell lines tested. Lig4 is essential for completion of the critical ligation step in c-NHEJ. In addition to low Lig4 expression, IMR32 and LAI-55n cells also had low expression of Artemis compared with fibroblasts, SH-EP1, SH-SY5Y, and SK-N-Be(2) cells. Artemis processes DNA terminal ends in the c-NHEJ pathway. These distinct NHEJ expression patterns, specifically upregulation of Lig3, Lig1, and PARP1 in cells with high-risk genotypes, along with deficiency of Lig4 and Artemis in IMR32 and LAI-55n cells, suggest that some high-risk neuroblastoma cells rely on alt-NHEJ rather than c-NHEJ for DSB repair.

alt-NHEJ ligases have not been previously linked to high-risk neuroblastoma. To determine whether a high-risk genetic alteration such as MNA controls alt-NHEJ ligase expression, we next evaluated expression of Lig3, Lig1, and Lig4 in SH-EP1 cells transfected to constitutively express MYCN. Transgene-induced expression of MYCN significantly increased both Lig3 and Lig1 protein expression in SH-EP1 cells, whereas Lig4 was unchanged from vector controls (Fig. 2B). High levels of MYCN expression were sufficient to increase alt-NHEJ ligase expression without changes in c-NHEJ factors (Lig4 or Ku70/80). These findings demonstrate a novel association between high-risk neuroblastoma and alt-NHEJ, highlighting a role for NHEJ in neuroblastoma pathogenesis.

Given these results, we next investigated whether MYCN expression could lower NHEJ accuracy. To determine differences in repair fidelity between MNA and non-MNA cells, we evaluated DSB repair by NHEJ plasmid end-joining in SH-EP1-MYCN cells and SH-EP1-vector controls. Transgene-induced expression of MYCN significantly decreased repair accuracy in SH-EP1 cells as measured by plasmid end-joining efficiency after BsrG1 and HindIII digestion (Fig. 2C). MYCN expression increased DSB repair error rates by 25%, with total error rates as high as 70% in SH-EP1-MYCN. These data link MYCN expression to an increase in DSB end-joining errors and provide a mechanism by which high-risk neuroblastoma cells may have propensity to generate misrepair events.

Inhibition of Lig3 and Lig1 increases DSB accumulation and induces cell death in neuroblastoma cells

High expression of alt-NHEJ ligases coupled with the near absence of Lig4 in high-risk neuroblastoma cells suggests that

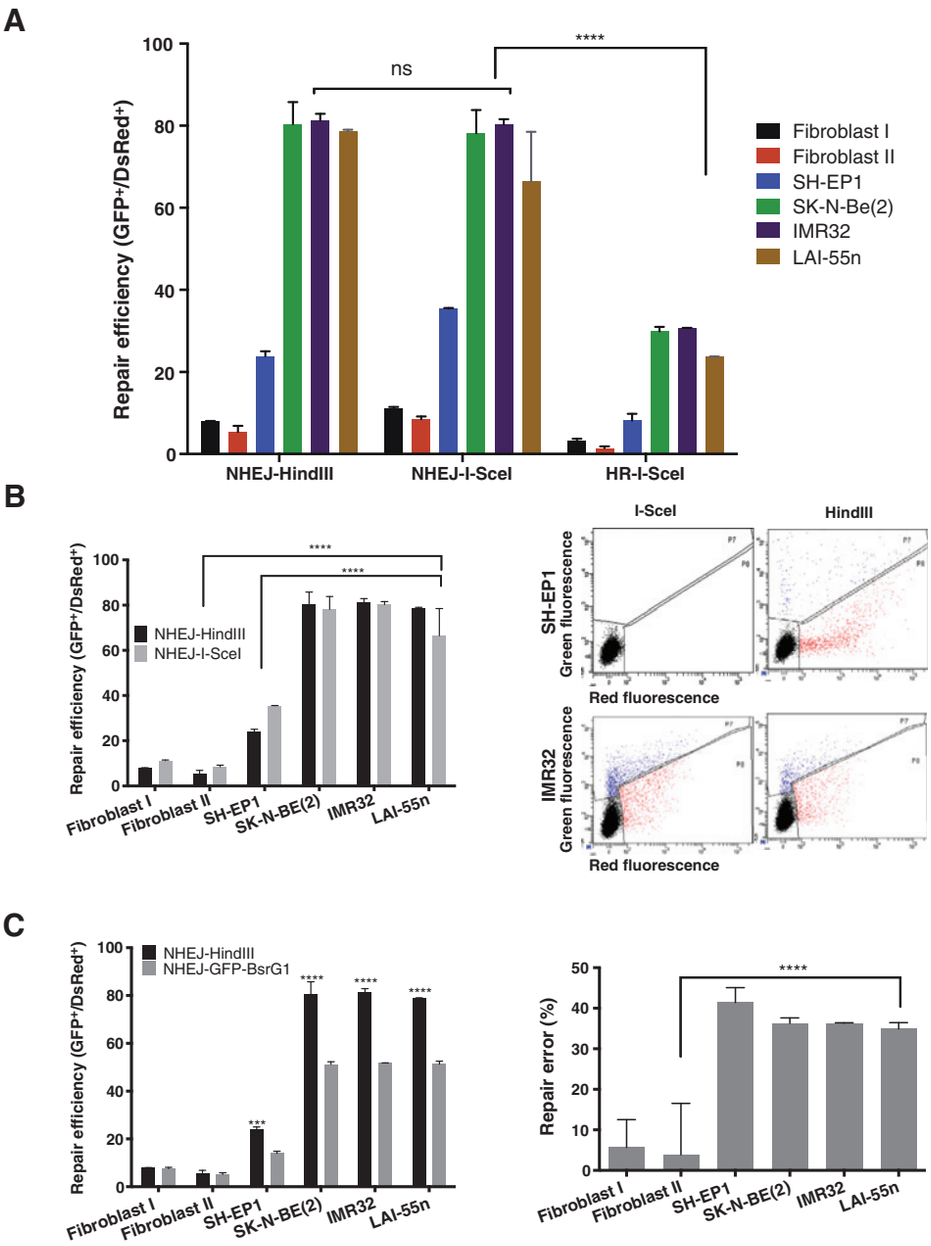

Figure 1.

A, NHEJ activity in neuroblastoma is efficient and error-prone. Utilizing sensitive fluorescent HR and NHEJ reporter constructs (Supplementary Figs. S1 and S2), DSB repair activity was measured in terms of successful reconstitution of GFP. Compared with HR, NHEJ was the most efficient mechanism of DSB repair across neuroblastoma cell lines (ANOVA used to test for differences between HR-I-SceI and NHEJ-I-SceI, and between NHEJ-HindIII and NHEJ-ISceI repair efficiencies for each cell line, **** significant at $P < 0.0001$; ns, not significant). NHEJ-Hind III and NHEJ-ISceI had similar repair activity, indicating that the same end-joining mechanism was likely responsible for repair of both compatible and incompatible DNA ends. NHEJ was most efficient in SK-N-Be(2), IMR32, and LAI-55n cells. There were no significant differences between HR and NHEJ repair efficiencies in the nontransformed fibroblast cell lines (both ANOVA and the Student *t* test used, $P = 0.07$). B, SK-N-Be(2), IMR32, and LAI-55n cells reached repair efficiency rates greater than 80% compared with fibroblasts I and II (IMR 90 and HFF-1) and stromal-type SH-EP1 cells, where repair efficiency was only 10% to 20% [ANOVA used to test for differences in NHEJ repair efficiencies between normal fibroblasts and each neuroblastoma cell line, **** significant at $P < 0.0001$, and for differences in NHEJ repair efficiencies between SH-EP1 and neuroblastic SK-N-Be(2), IMR32, and LAI-55n cells, **** significant at $P < 0.0001$]. Representative FACS-based plots showing IMR32 cells with increased green fluorescence population for both I-SceI and HindIII, indicating higher NHEJ activity compared with SH-EP1. C, NHEJ repair fidelity was determined utilizing NHEJ-GFP-BsrG1. Only accurate repair of BsrG1 digested pEGFP-PEM1 generated intact GFP, while Hind III tolerates microdeletions or addition of bases during the end-joining process. Plasmid rejoining in neuroblastoma cells had low fidelity with erroneous NHEJ repair products compared with normal fibroblasts. NHEJ activity in the entire panel of neuroblastoma cells was overall inaccurate with error rates ranging from 24% to 55% versus 0% to 5% in nontransformed cells. (ANOVA used to test for significant differences in repair efficiencies between NHEJ-HindIII and NHEJ-GFP-BsrG1 for each cell line, and for differences in repair error rates between normal fibroblasts and SH-EP1, SK-N-Be(2), IMR32, and LAI-55n; ***, $P < 0.001$; ****, $P < 0.0001$). Results are representative of three different experiments ± SEM.

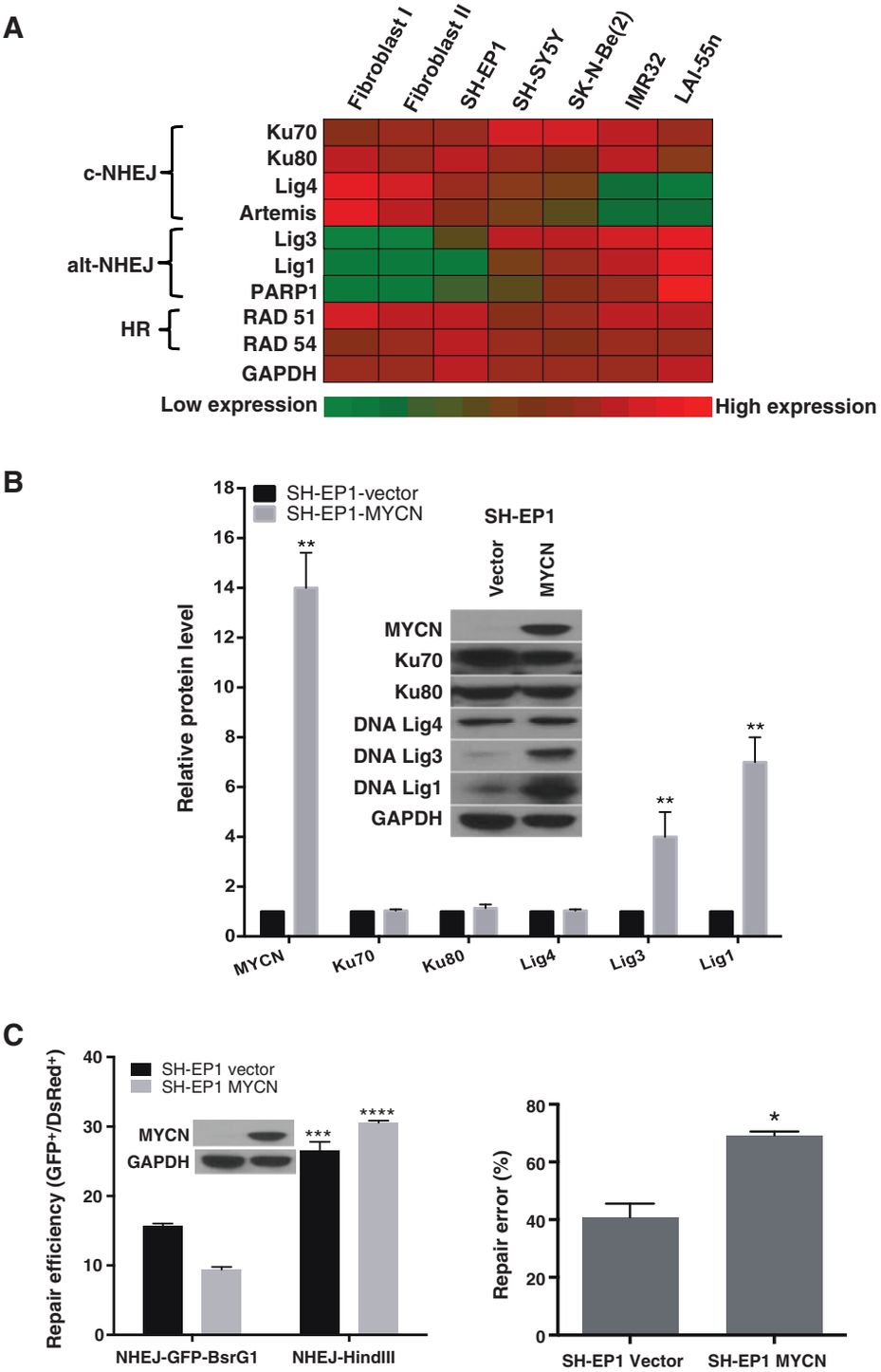

Figure 2.
A, neuroblastoma cell lines have differential NHEJ repair protein expression patterns. A heatmap plot was generated using conditional formatting in MS Excel and is based on protein expression quantification of Western blot analysis. Heatmap of representative immunoblot analysis (Supplementary Fig. S3) shows that neuroblastic neuroblastoma cells with high-risk genotypes [SH-SY5Y, SK-N-Be(2), IMR32, and LAI-55n] had differential NHEJ repair protein expression patterns compared with stromal-like SH-EP1 cells and to normal fibroblasts with upregulation of alt-NHEJ proteins (Lig3, Lig1, and PARP1) . In neuroblastic cells with MNA (IMR32, LAI-55n), there was downregulation of the c-NHEJ ligase, Lig4. IMR32 and LAN-55n cells also had low expression of Artemis compared with fibroblasts, SH-EP1, SH-SY5Y, and SK-N-Be(2) cells. GAPDH was used as loading control. Ku70/Ku80 and HR proteins (RAD 51 and RAD 54) were uniformly expressed across cell lines. B, immunoblot and protein quantification analysis using ImageJ software after transgene-induced expression of MYCN revealed increased alt-NHEJ ligases expression (Lig3, Lig1) in SH-EP cells while Lig4 was unchanged. GAPDH was used as loading control. C, NHEJ repair efficiency and fidelity was determined utilizing NHEJ-BsrG1 where only accurate repair of BsrG1 digested pGFP-PEM1 generates intact GFP. MYCN-transduced cells had a 25% increase in repair error, with error rates as high as 65% compared with 40% in SH-EP1-vector cells. Results are representative of three independent experiments ± SEM. Significant differences were analyzed with two-way ANOVA (*, $P = 0.014$; **, $P < 0.01$; ***, $P < 0.001$; ****, $P < 0.0001$).

DSB repair in this subset depends on alt-NHEJ. If so, inhibition of alt-NHEJ factors may impair DNA repair capacity in neuroblastoma cells. To test the hypothesis that high-risk neuroblastoma cells rely on alt-NHEJ for DSB repair, we utilized a Lig3 and Lig1 dual inhibitor to disrupt alt-NHEJ ligase function and measured the effects on DSB accumulation. L67 is a competitive inhibitor that specifically targets DSB repair by inhibiting alt-NHEJ ligases (Lig3 and Lig1) but does not affect c-NHEJ (Lig4; ref. 30). SH-EP1 (stromal-like), SH-SY5Y (neuroblastic, 1q trisomy), and IMR32 (neuroblastic, MNA and *1p* deletion) cells were examined as representative diverse phenotypes typical of neuroblastoma tumors. DSB accumulation was quantified by measuring phosphorylation of histone H2AX (γH2AX), a surrogate marker of nuclear DSB (31). Immunocytochemistry (ICC) was used to

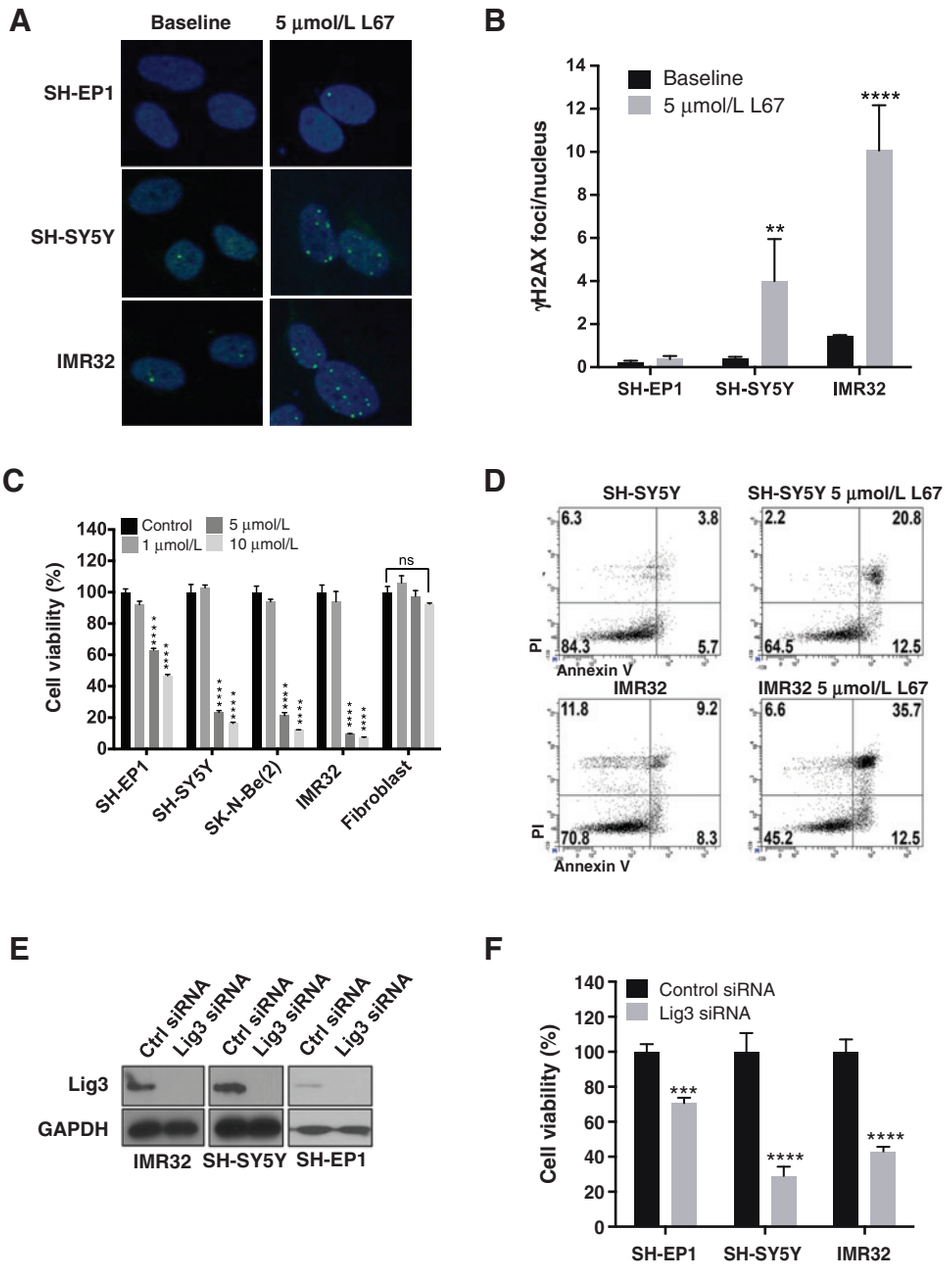

Figure 3.
Lig3 and Lig1 inhibition (L67) results in increased DSB accumulation and kills neuroblastoma cells. A, effects of L67 (5 μmol/L) on DSB accumulation were defined based on phosphorylation of γH2AX in SH-EP1, SH-SY5Y, and IMR32 and analyzed by ICC after 48-hour treatment. Shown is representative nuclear staining visualized using fluorescence microscopy (×40). B, γH2AX quantification analysis using ImageJ (400–500 cells were counted for each experiment). Compared with SH-EP1 (mean 0.2 foci/nucleus) and SH-SY5Y (mean 0.3 foci/nucleus), IMR32 (1.4 foci/nucleus, 7-fold higher than SH-EP1 and 4-6 fold higher than SH-SY5Y) had high endogenous DSB at baseline before treatment ($P < 0.0001$). Treatment with L67 (5 μmol/L) caused significant increases in γH2AX foci from baseline in SH-SY5Y ($P = 0.0070$) and in IMR32 cells ($P < 0.0001$). There were no significant changes in DSB accumulation in SH-EP1 cells ($P = 0.9975$). C, the effects of L67 (0 μmol/L, 1 μmol/L, 5 μmol/L, 10 μmol/L) on cell viability were tested in SH-EP1, SH-SY5Y, SK-N-BE2, IMR32 cells, and in normal fibroblasts (IMR90). Cell viability measured by the MTT assay at 48-hour treatment intervals were compared with vehicle control. neuroblastoma cell lines, particularly SH-SY5Y, SK-N-BE2, and IMR32 exhibited significant hypersensitivity to L67, while normal fibroblasts were not affected. D, cell death was detected by flow-cytometric analysis of Annexin V and PI with L67 (5 μmol/L). Representative FACS traces from SH-SY5Y and IMR32 after 48-hour treatment are shown with evidence of cells in both the early apoptotic stages (annexin V–positive, PI-negative), as well as nonviable, necrotic cells (annexin V–positive, PI-positive). E, siRNA knockdown of Lig3. Adequate Lig3 siRNA silencing was confirmed by Western blot analysis at 72 hours. F, cell survival after siRNA Lig3 was determined by the MTT viability assay after 72-hour exposure. SH-SY5Y and IMR32 cells had significantly decreased cell viability (60%–70%) compared with SH-EP1 cells (20%–25%). Results are representative of the mean of three independent experiments ± SEM. Significant differences were analyzed with ANOVA (**, $P < 0.01$; ***, $P = 0.001$; ****, $P < 0.0001$).

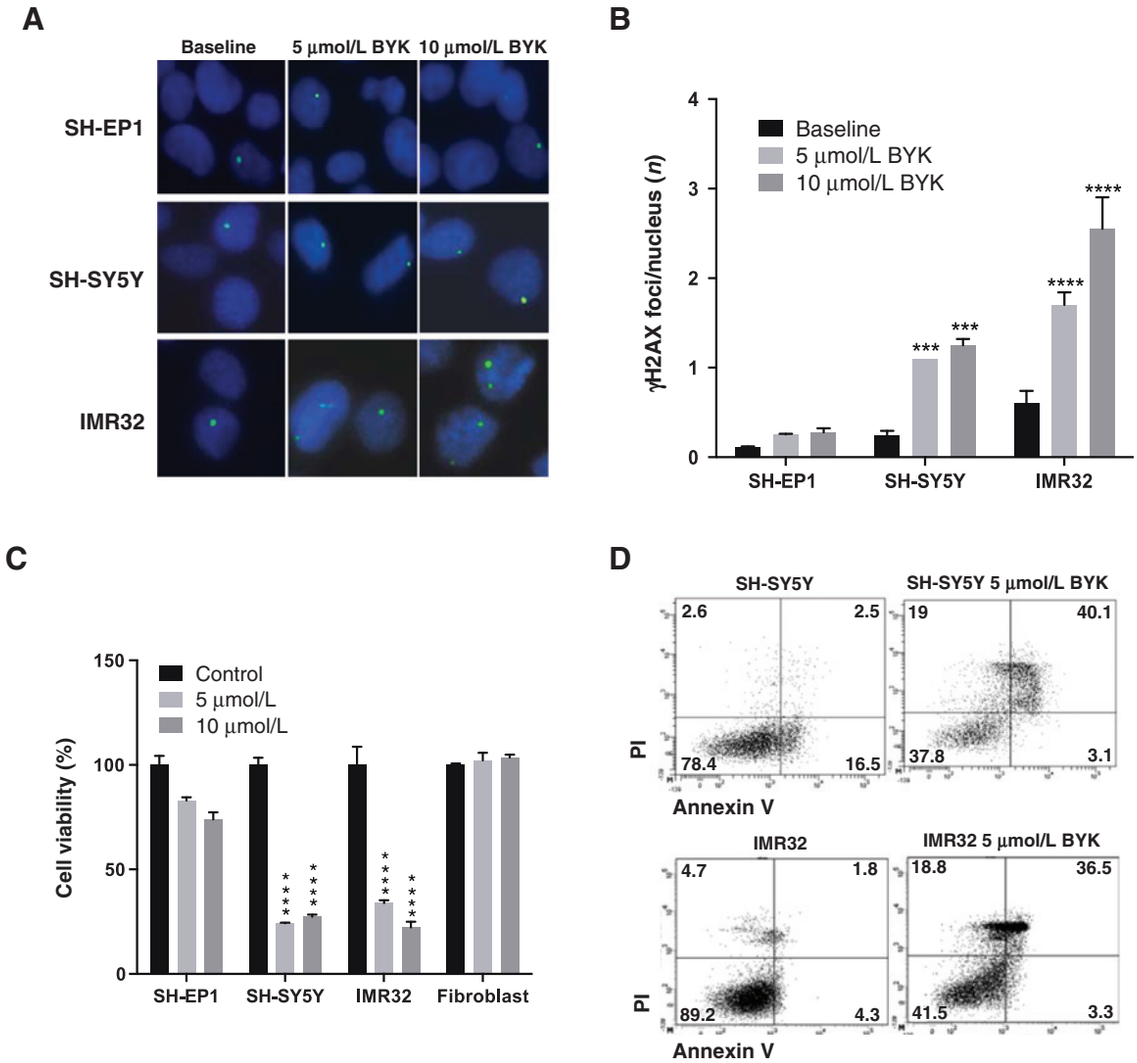

Figure 4.
PARP1 inhibition impairs DSB repair and kills neuroblastoma cells. A, effect of PARP1 inhibitor (BYK) on DSB accumulation in neuroblastoma cells was tested. DSB accumulation was measured by γH2AX after SH-EP1, SH-SY5Y, and IMR32 cells were treated with BYK (0 μmol/L, 5 μmol/L, 10 μmol/L) for 48 hours. Representative images were taken under fluorescence microscopy (×40) showing increased DSB accumulation in SH-SY5Y and IMR32 cells, with highest DSB accumulation detected in IMR32 cells after PARP1i. PARP1i did not affect DSB accumulation in SH-EP1 cells (400–500 cells were counted for each experiment). B, representative quantification of γH2AX foci. C, cell viability measured by the MTT assay after BYK (0 μmol/L, 5 μmol/L, 10 μmol/L) treatment for 48 hours revealed decreased viability in SH-SY5Y and IMR32 cells. PARP1i did not significantly affect SH-EP1 or fibroblast cell viability. D, cell death in both the early apoptosis stage and nonviable/necrotic stage were detected by flow cytometry after Annexin V and PI in the total cell population with BYK (5 μmol/L) at 48 hours. Representative SH-SY5Y and IMR32 data are shown. All data are expressed as the mean from three independent experiments. Significant differences were analyzed with ANOVA (***, $P < 0.001$; ****, $P < 0.0001$).

quantify γH2AX foci in the nuclei. IMR32 cells had high endogenous DSB before treatment compared with SH-EP1 and SH-SY5Y cells (Fig. 3A and B). Treatment with L67 induced a greater than 2-fold increase in γH2AX foci from baseline in SH-SY5Y and greater than 4-fold increase in IMR32. There was no significant increase in DSB accumulation in SH-EP1 cells after treatment with L67. These results imply that blocking Lig3 and Lig1 results in failure of DSB repair with DSB accumulation in neuroblastoma cells with high-risk genotypes. We reasoned that neuroblastic neuroblastoma cells utilize alt-NHEJ as a primary DNA repair mechanism and that DSB recovery is hindered by inhibiting alt-NHEJ ligases.

Because failure of DSB repair is a trigger for cell death, we further reasoned that since L67 selectively increased DSB accumulation, treatment with L67 similarly selectively induced cell death in high-risk neuroblastoma cell groups. Cell viability was measured by the MTT assay (Fig. 3C). Neuroblastoma cell lines were differentially hypersensitive to L67 killing while normal skin fibroblasts were insensitive. Neuroblastoma cell lines, particularly neuroblastic [SH-SY5Y, SK-N-Be(2), IMR32] cells were highly sensitive to L67, with significantly decreased cellular viability compared with untreated controls. To further differentiate the state of cell death, the Annexin V–FITC method was utilized. L67 (5 μmol/L) caused an increase in cell death in neuroblastoma cells

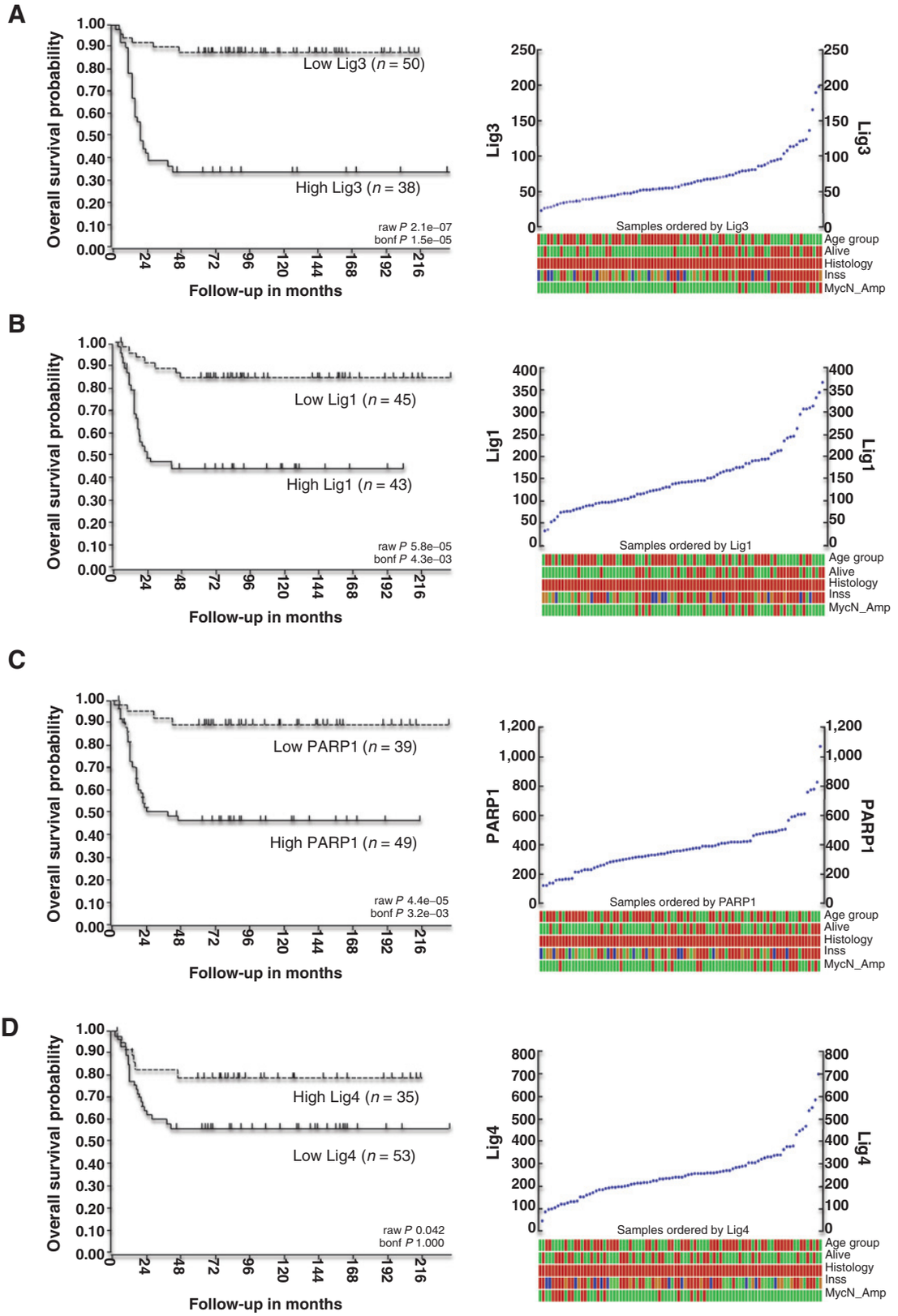

by 48 hours, as illustrated by flow-cytometric detection of Annexin V and PI, with detection of cells in both the early apoptotic stages as well as many nonviable, necrotic neuroblastoma cells (Fig. 3D).

To further test this hypothesis, we utilized siRNA to specifically knockdown Lig3 in SH-EP1, SH-SY5Y, and IMR32 cells. Mock transfection and transfection with scrambled siRNA served as controls. Western analysis using Lig3 antibodies 72 hours after transfection revealed significant Lig3 siRNA-induced knockdown compared with siRNA controls (Fig. 3E). Cell viability, assessed by Trypan blue exclusion showed that Lig3 knockdown in SH-SY5Y and in IMR32 cells caused a 60% to 70% decrease in cellular viability (Fig. 3F). Cleavage of PARP1 in this experiment was used as an indicator of apoptotic cell death (Supplementary Fig. S4). The change in viability in high-risk neuroblastic cells (SH-SY5Y and IMR32) was more than 2-fold the change observed with Lig3 depletion in SH-EP1 cells, where cellular viability was reduced by 20% to 25% from baseline. There were no changes in viability of neuroblastoma cells transfected with mock or scrambled siRNA control constructs. These data link loss of alt-NHEJ ligases to DSB accumulation and cell death in neuroblastoma cells and establish evidence of a functional role for alt-NHEJ in DSB repair and cell survival.

PARP1 inhibition increases DSB accumulation and kills neuroblastoma cells

To further define alt-NHEJ function in neuroblastoma, we studied the sensitivity of three neuroblastoma cell lines to PARP1 inhibition (PARPi) with BYK204165 (BYK), a potent and selective inhibitor of PARP1. PARP1 is a DSB-sensing and DNA-binding component in the alt-NHEJ pathway. PARP1 promotes mutagenic DSB repair by blocking c-NHEJ via Ku70 and Lig4 and participates in DSB repair in the absence of c-NHEJ (32, 33). We expected that PARPi would disrupt alt-NHEJ function and lead to a failure of DSB repair and cell death because inhibition of alt-NHEJ ligases caused DSB accumulation and cell death in neuroblastoma cells expressing alt-NHEJ proteins. To determine whether PARPi impaired DNA repair, phosphorylation of γH2AX foci was detected by ICC and measured in SH-EP1, SH-SY5Y, and IMR32 cells after treatment with BYK (0, 5, 10 μmol/L). In SH-SY5Y and IMR32 cells, BYK induced significant increases in nuclear γH2AX foci accumulation (Fig. 4A and B). DSB accumulation in IMR32 cells after PARPi was enhanced more than 2-fold higher than baseline vehicle controls. There were no differences in DSB accumulation after BYK in SH-EP1 cells suggesting that PARPi selectively blocks DSB recovery in neuroblastic neuroblastoma cells. SH-EP1, SH-SY5Y, and IMR32 cells were next treated with escalating doses of BYK (0, 5, 10 μmol/L) to determine the effects of PARPi on cell survival. Viability was measured by the MTT assay (Fig. 4C). SH-SY5Y and IMR32 cells were more sensitive to PARPi than SH-EP1 cells and fibroblasts, with decreased viability and significantly increased cell death (Fig. 4D). PARPi in SH-SY5Y and IMR32 cells resulted in more than 75% decrease in cell viability compared with SH-EP1 cells (25%) while fibroblasts were relatively insensitive to BYK. These results provide further mechanistic evidence that components of alt-NHEJ are critical for DSB recovery and cell viability in neuroblastoma. Because selective inhibition of key alt-NHEJ mediators (Lig3/Lig1 and PARP1) is selectively cytotoxic to neuroblastic and MNA neuroblastoma cells, these findings set precedence for targeting alt-NHEJ in neuroblastoma tumors with high-risk phenotypes.

Expression of NHEJ genes in neuroblastoma tumors correlate with patient outcome

Because NHEJ proteins had distinct expression patterns in cultured high-risk neuroblastoma cells, we questioned whether high-risk neuroblastoma tumors have high expression of alt-NHEJ genes and how alt-NHEJ expression levels might correlate with patient survival. Here, we examined expression of NHEJ genes in patient tumor samples from a publically available database (Academic Medical Center cohort; GEO database accession no. GSE16476). We studied NHEJ gene expression in 88 diverse human neuroblastoma samples in the Web-based R2 microarray database (http://hgserver1.amc.nl/cgi-bin/r2/main.cgi) to determine Lig3, Lig1, Lig4, and PARP1 expression levels. High expression of Lig3 significantly associated with poor patient survival (Fig. 5A). Overall, 38 patients had high Lig3 expression levels and 50 patients had low Lig3 expression. Low Lig3 expression correlated with excellent long-term patient survival and overall survival probability of 88%, whereas high expression reduced overall survival probability to 34%, and was associated with older age at presentation (>18 mo), higher stage disease, and MNA. Similarly, patients with high expression of Lig1 had worse overall survival probabilities and higher stage disease than those with low Lig1 (Fig. 5B). The overall survival probability in patients with high Lig1 expression was 44% versus 84% in patients with low Lig1 expression. High PARP1 was also associated with worse overall survival probability and higher disease stage (Fig. 5C). Tumors with high expression of the c-NHEJ ligase, Lig4 was associated with significantly higher survival probabilities (79%) compared with patients with low Lig4 transcripts (56%; Fig. 5D). Importantly, tumors with low Lig4 expression were associated with higher stage disease and MNA. Variation of alt-NHEJ gene expression in patients with worse survival outcomes reflects known heterogeneity in neuroblastoma tumors and may

Figure 5.

The expression of NHEJ components predicts clinical outcome in neuroblastoma patients. Kaplan–Meier survival curves and outcome data histograms were downloaded from the R2 microarray analysis and visualization platform based on expression of several NHEJ genes in a diverse panel of neuroblastoma tumors ($n = 88$). The R2 microarray analysis platform was used for analysis and is the source of data. Scan modus was used for cutoff determination with a minimum group size of 10 to determine the best P value, and P values were corrected for multiple testing (Bonferroni). Gene expression was correlated with survival, age group (<18 months = red, >18 months = green), alive (no = red, yes = green), INSS stage (stage IV = red, III = orange, I/II = green, IVs = blue) and MNA (MYCN-Amp = red, non-MYCN-Amp = green). A, Kaplan–Meier curve and expression plot revealed that high Lig3 expression had worse overall survival probability (34%) compared with patients with low Lig3 expression (88%), cutoff 64.6, $P = 2.1e\text{-}07$. Lig3 was highly expressed in stage IV and MNA tumors and was also associated with patients over 18 months of age. Both high Lig1 (B) and PARP1 (C) expression also correlated with poor overall survival probabilities (44% for Lig1, cutoff 141.1, $P = 5.8e\text{-}05$, 46% for PARP1, cutoff 341.5, $P = 4.4e\text{-}05$) and higher stage disease without correlation to MNA or age. D, patients with tumors expressing low Lig4 had worse overall survival probabilities compared with those with tumors expressing high Lig4 (56% vs. 79%, cutoff 258.1, $P = 0.042$) and correlated with higher stage disease and MNA. Thus high alt-NHEJ ligase and PARP1 expression correlate with poor overall patient survival and high-risk tumor phenotypes while high Lig4 was associated improved survival, lower stage disease, and non-MNA tumors.

contribute to biologic diversity in this disease. These findings highlight a subgroup of neuroblastoma patients that may benefit from development of therapeutics targeting NHEJ pathways.

Discussion

There is increasing evidence that deregulation of NHEJ is a pathogenic factor in a number of cancers, including breast cancer, chronic myelogenous leukemia (CML), and soft-tissue sarcomas (34–38). Our results provide new evidence that NHEJ is deregulated in neuroblastoma and provide explanation for the increased propensity of neuroblastoma tumors to harbor pathogenic segmental chromosomal alterations. Our initial observation that efficient but erroneous NHEJ repair is the dominant DSB repair pathway utilized by neuroblastoma cells with high-risk genotypes led us to question whether there are differences in protein and gene expression of key NHEJ factors. This distinct NHEJ expression pattern, with neuroblastoma cells that harbor chromosomal alterations having high levels of alt-NHEJ factors and low levels of major c-NHEJ factors, provides a unique survival advantage for neuroblastoma cells that have not been previously explored. The clinical relevance of these results is grounded in our finding that patients with neuroblastoma tumors that overexpress alt-NHEJ genes have higher stage disease and worse survival outcomes. These experimental results offer a new mechanistic model for neuroblastoma pathogenesis in which high-risk neuroblastoma cells survive DNA damage by upregulation of an efficient but erroneous alt-NHEJ pathway. Because alt-NHEJ is distinguished by low-fidelity repair that is characterized by deletions and unbalanced translocations, the overall result is neuroblastoma DNA maintenance with repair products that are prone to generate segmental chromosomal errors. Alternatively, as we detected in IMR32 cells, neuroblastoma cells with high-risk genotypes may have high endogenous levels of DSB compared with lower-risk cells, and by an efficient alt-NHEJ repair mechanism, erroneous repair is the result of abnormally high levels of DSB repair events.

How neuroblastoma cells regulate NHEJ is a compelling question. One explanation is that genes within the *MYC* family have recently been implicated in the regulation of DSB repair pathways, though this is the first report linking MYCN to NHEJ (39). In our study, transgene expression of MYCN increased alt-NHEJ ligase expression resulting in impaired NHEJ fidelity, while by expression of the c-NHEJ ligase, Lig4 was not affected. This implies that neuroblastoma cells with MNA preferentially upregulate alt-NHEJ ligases. If so, these data further clarify the pathways by which neuroblastoma tumors with MNA develop mechanisms to circumvent DNA damage and evade cell death signals (40). Compared with stromal-like neuroblastoma cells, MYCN-expressing cells fail to undergo G_1 arrest after DNA damage (41). This is due to lower levels of *CDKN1A* ($p21^{WAF1}$), a potent cyclin-dependent kinase inhibitor that regulates cell-cycle progression at G_1 and S phases (42). Without an adequate G_1 checkpoint, an efficient DNA repair mechanism is a critical component of MYCN-expressing neuroblastoma cell survival as cells are forced to rapidly progress through the cell cycle. We reason that *MYCN*-linked enhancement of alt-NHEJ contributes to an inherent capacity of neuroblastoma cells to overcome DNA damage efficiently under stress of fast replication while avoiding checkpoint death signals.

The most significant findings from our work are that alt-NHEJ may represent a new therapeutic target for patients with high-risk neuroblastoma tumors. There is an immediate need to develop improved therapies for children with neuroblastoma refractory to current therapies. Targeting alt-NHEJ in select cancers is a promising therapeutic strategy for patients who fail conventional treatment modalities (36, 37). The recent success of PARP1 inhibitors in clinical trials for select solid tumors has also given promise to alternative DNA repair mechanisms as cancer-specific therapeutics (43). Our experimental data suggest that alt-NHEJ inhibition in neuroblastoma cells with high-risk features hinders an adequate DNA damage response and incites nuclear DSB accumulation and cell death. There are consistent differences in NHEJ factor expression at the protein and mRNA levels. This is illustrated by the finding that compared with nontransformed cells and stromal-like SH-EP1 cells, a subset of neuroblastic neuroblastoma cells with segmental chromosomal alterations has a predictable alt-NHEJ protein expression pattern with high levels of Lig3, Lig1, and PARP1, and low levels of c-NHEJ proteins, Lig4 and Artemis. Moreover, patients with neuroblastoma tumors that overexpress Lig3, Lig1, and PARP1 have overall poor survival compared with patients with low expression. Given this, NHEJ expression patterns of neuroblastoma tumors may be useful to predict which patients are likely to benefit from alt-NHEJ pathway inhibition.

In addition to its nuclear functions, Lig3 is also present in mitochondria of mammalian cells, where until recently its biologic role was unclear. Recent studies have discovered that Lig3 deficiency does not result in nuclear DNA repair deficiency but loss of mitochondrial DNA integrity (44–46). This indicates that in cells with an intact c-NHEJ pathway, essential nuclear repair functions can occur in the absence of Lig3 but that mitochondrial DNA repair is compromised. The precise viability requirement (nuclear or mitochondrial) of Lig3 and alt-NHEJ that we discovered in neuroblastoma requires further study, though with alt-NHEJ inhibition, nuclear DSB increased. Additional experimental analyses are therefore required to determine the effect of alt-NHEJ inhibition on mitochondrial DNA integrity compared with nuclear DNA in cancer cells, particularly in neuroblastoma cells. In our current studies, inhibition of alt-NHEJ factors did not significantly affect nontransformed human fibroblasts. This indicates that blocking DSB repair by alt-NHEJ may be a cancer cell-specific strategy that has potential to minimize toxicity to nuclear DNA of normal cells.

Targeting a major DSB repair pathway would provide opportunity for a paradigm shift in treatment options for patients with high-risk neuroblastoma because radiotherapy and common chemotherapies induce DSB, rather than inhibit DNA repair pathways (47). Collectively, the current data are evidence that alt-NHEJ is functional in neuroblastoma pathogenicity and offer experimental support for preclinical studies targeting NHEJ pathways in high-risk neuroblastoma tumors.

Disclosure of Potential Conflicts of Interest

No potential conflicts of interest were disclosed.

Authors' Contributions

Conception and design: E.A. Newman, A.W. Opipari, V.P. Castle
Development of methodology: E.A. Newman, A.W. Opipari, V.P. Castle
Acquisition of data (provided animals, acquired and managed patients, provided facilities, etc.): E.A. Newman, F. Lu, D. Bashllari
Analysis and interpretation of data (e.g., statistical analysis, biostatistics, computational analysis): E.A. Newman, F. Lu, D. Bashllari, A.W. Opipari, V.P. Castle

Writing, review, and/or revision of the manuscript: E.A. Newman, D. Bashllari, A.W. Opipari, V.P. Castle
Administrative, technical, or material support (i.e., reporting or organizing data, constructing databases): E.A. Newman
Study supervision: E.A. Newman, V.P. Castle
Other (performed the preliminary data to generate the hypothesis for this study): L. Wang

Acknowledgments

The authors thank Drs. Elizabeth Lawlor and Mats Ljungman for insightful comments and for careful reading of the article, and Dr. Chitra Subramarian for help with the initial Lig3 siRNA knockdown experiments.

Grant Support

This work was financially supported in part by funds from the Robert Wood Johnson Foundation/Amos Medical Faculty Development Program (to E.A. Newman), The Alfred Taubman Medical Research Institute/Edith Briskin Emerging Scholar Program (to E.A. Newman, VP Castle), and the Section of Pediatric Surgery, The University of Michigan (to E.A. Newman).

The costs of publication of this article were defrayed in part by the payment of page charges. This article must therefore be hereby marked *advertisement* in accordance with 18 U.S.C. Section 1734 solely to indicate this fact.

Received June 13, 2014; revised November 17, 2014; accepted December 7, 2014; published OnlineFirst January 6, 2015.

References

1. Brodeur GM, Seeger RC, Schwab M, Varmus HE, Bishop JM. Amplification of N-myc in untreated human neuroblastomas correlates with advanced disease stage. Science 1984;224:1121–4.
2. Seeger RC, Brodeur GM, Sather H. Association of multiple copies of the N-myc oncogene with rapid progression of neuroblastomas. NEJM 1985; 313:1111–6.
3. Janoueix-Lerosey I, Schleiermacher G, Michels E, Mosseri V, Ribeiro A, Lequin D, et al. Overall genomic pattern is a predictor of outcome in neuroblastoma. J Clin Oncol 2009;27:1026–33.
4. Schleiermacher G, Janoueix-Lerosey I, Ribeiro A, Klijanienko J, Couturier J, Pierron G, et al. Accumulation of segmental alterations determines progression in neuroblastoma. J Clin Oncol 2010;28:3122–30.
5. Maris JM, Hogarty MD, Bagatell R, Cohn SL. Neuroblastoma. Lancet 2007; 369:2106–20.
6. Attiyeh EF, London WB, Mossé YP, Wang Q, Winter C, Khazi D, et al. Chromosome 1p and 11q deletions and outcome in neuroblastoma. N Engl J Med 2005;353:2243–53.
7. Luttikhuis M, Powell JE, Rees SA, Genus T, Chughtai S, Ramani P, et al. Neuroblastomas with chromosome 11q loss and single copy MYCN comprise a biologically distinct group of tumours with adverse prognosis. Br J Cancer 2001;85:531–7.
8. Vandesompele J, Baudis M, De Preter K, Van Roy N, Ambros P, Bown N, et al. Unequivocal delineation of clinicogenetic subgroups and development of a new model for improved outcome prediction in neuroblastoma. J Clin Oncol 2005;23:2280–99.
9. Spitz R, Hero B, Ernestus K, Berthold F. Deletions in chromosome arms 3p and 11q are new prognostic markers in localized and 4s neuroblastoma. Clin Cancer Res 2003;9:52–8.
10. èastowska M, Viprey V, Santibanez-Koref M, Wappler I, Peters H, Cullinane C, et al. Identification of candidate genes involved in neuroblastoma progression by combining genomic and expression microarrays with survival data. Oncogene 2007;26:7432–44.
11. Selzer RR, Richmond TA, Pofahl NJ, Green RD, Eis PS, Nair P, et al. Analysis of chromosome breakpoints in neuroblastoma at sub-kilobase resolution using fine-tiling oligonucleotide array CGH. Genes Chromosom Cancer 2005;44:305–19.
12. Stallings RL, Yoon K, Kwek S, Ko D. The origin of chromosome imbalances in neuroblastoma. Cancer Genet Cytogenet 2007;176:28–34.
13. Schleiermacher G, Mosseri V, London WB, Maris JM, Brodeur GM, Attiyeh E, et al. Segmental chromosomal alterations have prognostic impact in neuroblastoma: a report from the INRG project. Br J Cancer 2012;107: 1418–22.
14. Roth DB, Porter TN, Wilson JH. Mechanisms of nonhomologous recombination in mammalian cells. Mol Cell Biol 1985;5:2599–607.
15. Mao Z, Bozzella M, Seluanov A, Gorbunova V. Comparison of nonhomologous end joining and homologous recombination in human cells. DNA Repair 2008;7:1765–71.
16. Deriano L, Roth DB. Modernizing the nonhomologous end-joining repertoire: alternative and classical NHEJ share the stage. Annu Rev Genet 2013;47:433–55.
17. Moore JK, Haber JE. Cell cycle and genetic requirements of two pathways of nonhomologous end-joining repair of double-strand breaks in Saccharomyces cerevisiae. Mol Cell Biol 1996;16:2164–73.
18. Bogue MA, Wang C, Zhu C, Roth DB. V(D)J recombination in Ku86-deficient mice: distinct effects on coding, signal, and hybrid joint formation. Immunity 1997;7:37–47.
19. Liang F, Romanienko PJ, Weaver DT, Jeggo PA, Jasin M. Chromosomal double-strand break repair in Ku80-deficient cells. Proc Natl Acad Sci U S A 1996;93:8929–33.
20. Göttlich B, Reichenberger S, Feldmann E, Pfeiffer P. Rejoining of DNA double-strand breaks *in vitro* by single-strand annealing. Eur J Biochem 1998;258:387–95.
21. Wang H. DNA ligase III as a candidate component of backup pathways of nonhomologous end joining. Cancer Res 2005;65:4020–30.
22. Audebert M, Salles B, Calsou P. Involvement of poly(ADP-ribose) polymerase-1 and XRCC1/DNA ligase III in an alternative route for DNA double-strand breaks rejoining. J Biol Chem 2004;279:55117–26.
23. Yu AM, McVey M. Synthesis-dependent microhomology-mediated end joining accounts for multiple types of repair junctions. Nucleic Acids Res 2010;38:5706–17.
24. Simsek D, Jasin M. Alternative end-joining is suppressed by the canonical NHEJ component Xrcc4–ligase IV during chromosomal translocation formation. Nat Struct Mol Biol. Nature Publishing Group; 2010;17: 410–6.
25. Zhang Y, Gostissa M, Hildebrand DG, Becker MS, Boboila C, Chiarle R, et al. The role of mechanistic factors in promoting chromosomal translocations found in lymphoid and other cancers. Adv Immunol 2010;106: 93–133.
26. Molenaar JJ, Koster J, Zwijnenburg DA, van Sluis P, Valentijn LJ, van der Ploeg I, et al. Sequencing of neuroblastoma identifies chromothripsis and defects in neuritogenesis genes. Nature 2012;483:589–93.
27. Seluanov A. DNA end joining becomes less efficient and more error-prone during cellular senescence. Proc Natl Acad Sci 2004;101:7624–9.
28. Mao Z, Jiang Y, Liu X, Seluanov A, Gorbunova V. DNA repair by homologous recombination, but not by nonhomologous end joining, is elevated in breast cancer cells. Neoplasia (New York, NY) 2009;11:683–91.
29. Thiele CJ. Neuroblastoma cell lines. In: Masters J, editor. Human Cell Culture. Lancaster, UK: Kluwer Academic; 1998. Vol. 1, p. 21–53.
30. Chen X, Zhong S, Zhu X, Dziegielewska B, Ellenberger T, Wilson GM, et al. Rational design of human DNA ligase inhibitors that target cellular DNA replication and repair. Cancer Res 2008;68:3169–77.
31. Sedelnikova OA, Rogakou EP, Panyutin IG, Bonner WM. Quantitative detection of 125IdU-induced DNA double-strand breaks with γ-H2AX antibody. Radiation Res 2002;158:486–92.
32. Wang M, Wu W, Wu W, Rosidi B, Zhang L, Wang H, et al. PARP-1 and Ku compete for repair of DNA double strand breaks by distinct NHEJ pathways. Nucleic Acids Res 2006;34:6170–82.
33. Paddock MN, Bauman AT, Higdon R, Kolker E, Takeda S, Scharenberg AM. Competition between PARP-1 and Ku70 control the decision between high-fidelity and mutagenic DNA repair. DNA Repair 2011;10:338–43.
34. Zhu C, Mills KD, Ferguson DO, Lee C, Manis J, Fleming J, et al. Unrepaired DNA breaks in p53-deficient cells lead to oncogenic gene amplification subsequent to translocations. Cell 2002;109:811–21.
35. Difilippantonio MJ, Zhu J, Chen HT, Meffre E, Nussenzweig MC, Max EE, et al. DNA repair protein Ku80 suppresses chromosomal aberrations and malignant transformation. Nature 2000;404:510–4.

36. Tobin LA, Robert C, Rapoport AP, Gojo I, Baer MR, Tomkinson AE, et al. Targeting abnormal DNA double-strand break repair in tyrosine kinase inhibitor-resistant chronic myeloid leukemias. Oncogene 2013;32: 1784–93.
37. Sallmyr A, Tomkinson AE, Rassool FV. Up-regulation of WRN and DNA ligase IIIalpha in chronic myeloid leukemia: consequences for the repair of DNA double-strand breaks. Blood 2008;112: 1413–23.
38. Tobin LA, Robert C, Nagaria P, Chumsri S, Twaddell W, Ioffe OB, et al. Targeting abnormal DNA repair in therapy-resistant breast cancers. Mol Cancer Res 2012;10:96–107.
39. Chen Y, Xu J, Borowicz S, Collins C, Huo D, Olopade OI. c-Myc activates BRCA1 gene expression through distal promoter elements in breast cancer cells. BMC Cancer 2011;11:246.
40. Hogarty MD. The requirement for evasion of programmed cell death in neuroblastomas with MYCN amplification. Cancer Lett 2003;197: 173–9.
41. McKenzie PP, Guichard SM, Middlemas DS, Ashmun RA, Danks MK, Harris LC. Wild-type p53 can induce p21 and apoptosis in neuroblastoma cells but the DNA damage-induced G1 checkpoint function. Clin Cancer Res 1999;5:4199–207.
42. Mergui X, Leteurtre F, Lipinski M, Bénard J, Amor-Guéret M. Two distinctly altered cellular responses to DNA double-strand breaks in human neuroblastoma. Biochimie 2008;90:1656–66.
43. Curtin NJ. Inhibiting the DNA damage response as a therapeutic manoeuvre in cancer. Br J Pharmacol 2013;169:1745–65.
44. Simsek D, Furda A, Gao Y, Artus J, Brunet E, Hadjantonakis A-K, et al. Crucial role for DNA ligase III in mitochondria but not in Xrcc1-dependent repair. Nature 2011;471:245–8.
45. Simsek D, Brunet E, Wong SY-W, Katyal S, Gao Y, McKinnon PJ, et al. DNA ligase III promotes alternative nonhomologous end-joining during chromosomal translocation formation. Haber JE, editor. PLoS Genet 2011;7: e1002080.
46. Gao Y, Katyal S, Lee Y, Zhao J, Rehg JE, Russell HR, et al. DNA ligase III is critical for mtDNA integrity but not Xrcc1-mediated nuclear DNA repair. Nature. Nature Publishing Group; 2011;471:240–4.
47. Lieberman HB. DNA damage repair and response proteins as targets for cancer therapy. Curr Med Chem 2008;15:360–7.